Canadian Conference - Pacific Conference on Earthquake Engineering 2023
Vancouver, British Columbia
June 25th – June 30th, 2023

Residual Seismic Capacity of Damaged Reinforced Concrete Walls with Unconfined Boundaries

Edgar Chacón-Valero[1*], Matías Hube[2,3] and Hernán Santa María[2,3]

[1]PhD Student, Department of Structural and Geotechnical Engineering, Pontificia Universidad Católica de Chile, Santiago, Chile
[2]Researcher, National Research Center for Integrated Natural Disaster Management (GIGIDEN), ANID/FONDAP/1522A0005, Santiago, Chile
[3]Associate Professor, Department of Structural and Geotechnical Engineering, Pontificia Universidad Católica de Chile, Santiago, Chile
[*]eechacon@uc.cl (Corresponding Author)

ABSTRACT

Reinforced concrete (RC) wall buildings are widely used in areas of intense seismicity, providing high levels of lateral strength and stiffness. Earthquakes and aftershocks can lead to the accumulation of damage in the walls of these buildings. The extent of damage accumulation in these walls and their ability to preserve good seismic performance levels when subjected to strong and long-duration subduction earthquakes, i.e., their Residual Seismic Capacity (RSC), are likely unknown. Hence, assessing the RSC of RC walls with different levels of prior damage is relevant to overcome the technical drawbacks of the post-earthquake repair/demolish decision-making process. This paper summarizes an experimental campaign aimed to evaluate the RSC of rectangular, slender, and unconfined walls with different levels of prior damage. Four specimens, identical in geometry and materials, were constructed and tested under different quasi-static and displacement-controlled loading protocols. The walls had a shear-to-span ratio of 2.5, and a 10% axial load ratio. The first wall (benchmark) was tested undamaged using a standard Failure Loading Protocol (FLP). The remaining walls were previously loaded with a Damage Loading Protocol (DLP) with thirty cycles at 1.33, 1.66, and 2.00% target drift ratios, respectively. These walls were subsequently driven to failure by the FLP. Due to the 1.33% DLP, the specimen showed slight damage and loss of initial stiffness. The 1.66% DLP yielded the longitudinal and transverse reinforcement and provoked loss of the cover concrete. This specimen lost approximately 73% of its initial stiffness and 13% of its peak strength. The 2.00% DLP was associated with heavy damage and failure of the specimen before the end of the protocol. It is concluded that damaging protocols with drift ratios that at least quadrupled the drift at yielding of the walls affected the RSC of the studied specimens.

Keywords: Residual Seismic Capacity, Reinforced Concrete, Damage Walls, Seismic Performance.

INTRODUCTION

Quite often, earthquakes and aftershocks cause damage to Reinforced Concrete (RC) walls of buildings located in high seismically hazard regions. The extent of this damage and the ability of the walls to preserve good seismic performance (SP) levels when are subjected to significant earthquakes, i.e., their Residual Seismic Capacity (RSC), are mostly unknown. Lessons learned from recent earthquakes, e.g., Chile (2010), New Zealand (2011), Mexico (2017), and Turkey-Syria (2023) highlight the relevance of quickly determining the extent of damaged and the future SP of the structures located in regions with high seismic hazard [1]–[5]. Especially when the structural elements, such as slender and unconfined walls, are not expected to show high levels of ductility in significant earthquakes demands. Hence, assessing the RSC of walls with different levels of prior damage is a relevant matter for the post-earthquake repair/demolish decision-making process.

RSC can be understood as the ability of a damaged structural component to resist subsequent earthquakes. It is often quantified through parameters like change in stiffness, strength, energy dissipation, and fatigue resistance [6]. Several studies conducted on RC walls with different loading protocols, axial load ratios (ALR), boundary confinement patterns, reinforcing steel, and

shear-to-span ratios, report their SP when are tested from undamaged condition [7]–[14]. However, there are limited studies reported in the literature that evaluate the SP through estimating the RSC of damaged RC walls [15]–[17].

As a contribution to understand the mechanisms governing the SP of damaged RC walls, this paper summarizes an experimental campaign aimed to evaluate the RSC of rectangular, slender, and unconfined walls with different levels of prior damage. Four specimens, identical in geometry and materials, were constructed and tested under different quasi-static and displacement-controlled loading protocols. The walls had a shear-to-span ratio of 2.5, and a 10% axial load ratio. The first wall (benchmark) was tested undamaged using a standard Failure Loading Protocol (FLP). The remaining walls were previously loaded with a Damage Loading Protocol (DLP) with thirty cycles at 1.33, 1.66, and 2.00% target drift ratios, respectively. These walls were subsequently driven to failure by the FLP. The hysteretic behavior of the priorly damaged walls is described in this paper, including the visual damage evolution during the tests. In addition, the RSC of the damaged walls subjected to the FLP is quantified by estimating the FEMA component modification factors. Finally, results are discussed, and conclusions are drawn regarding the effect of the prior DLPs in the RSC of the damaged RC walls.

EXPERIMENTAL PROGRAM

Description of the wall specimens

The experimental walls are four 1/2 scale slender, rectangular, and unconfined walls. The base (foundation) of the prototype wall is 1800 mm long, 500 mm wide, and 750 mm high. The wall is 900 mm long, 2000 mm high, and 150 mm thick. Finally, the top beam is 90 mm long, 350 mm wide, and 500 mm high (Figure 1a). All specimens had a shear-to-span ratio (M/VL_w) of 2.5. The reinforcing steel of the walls is detailed as follows. Longitudinal boundary reinforcement consists of (2+2) ϕ12 mm (ρ_b = 0.44%). Longitudinal web reinforcement consists of 6 ϕ8 mm, distributed in two layers of three bars spaced 170 mm apart (ρ_l = 0.39%). Horizontal web reinforcement is provided by 2 ϕ6 mm hoops 150 mm spaced along the height of the wall, comprising a web reinforcement ratio, ρ_v = 0.25% (Figure 1b). Horizontal hoops consist of two opposed bars with 90-degree hooks embracing the vertical boundary reinforcement, but not anchored into the concrete core.

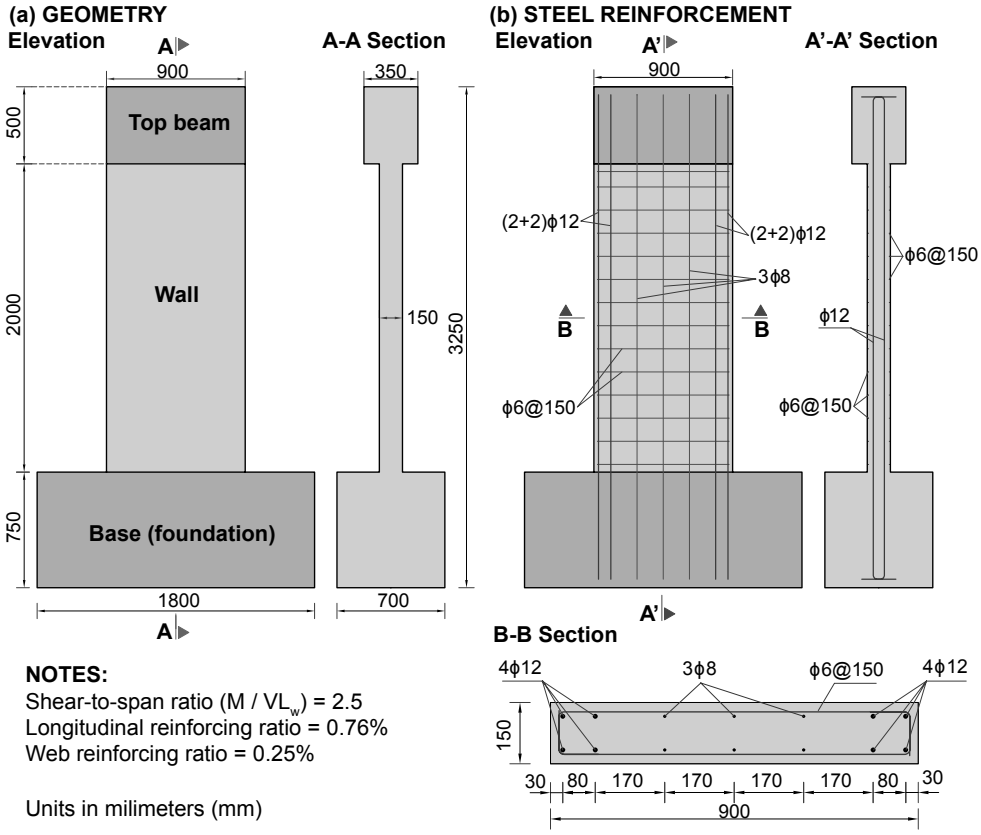

Figure 1. Prototype wall: (a) geometry, (b) steel reinforcement.

Materials

The average concrete compressive strength at the time of tests was 29.6 MPa. Average concrete elastic modulus (E_c) was experimentally determined according to ASTM C469 [18], E_c = 26900 MPa. The specified steel for bars ϕ12 and, ϕ8 mm was A630-420H [19] (f_y = 420 MPa) and for ϕ6 mm bars, ADN 420 (f_y = 420 MPa). The mechanical properties of ϕ12 mm bars were experimentally determined according to NCh200.Of1972 [20]. The mechanical properties of the ϕ6, and ϕ8 mm bars were taken from two previous experimental campaigns that used the same steel bars, [15], [21]. Table 1 summarizes the mechanical properties of the steel reinforcement of the wall specimens. In Table 1, d_b is the diameter of the steel bar, f_y is the tensile strength at yielding of the steel, f_u is the ultimate tensile strength, E_s is the elastic modulus of the steel, ε_y is the strain at yielding of the steel, and ε_u is the ultimate strain.

Table 1. Mechanical properties of the steel reinforcement.

Bars	d_b (mm)	f_y (MPa)	f_u (MPa)	E_s (MPa)	ε_y (%)	ε_u (%)
ϕ6*	6	493	700	200	0.25	18
ϕ8*	8	513	775	202	0.25	13
ϕ12	12	457	742	184	0.25	11

*: from [15].

Test setup and instrumentation

Lateral displacements were applied with the horizontally mounted hydraulic actuator anchored in the reaction wall shown in Figure 2(a). Out-of-plane displacements were restrained by a steel strut anchored in a second reaction wall (Figure 2b). The experimental set-up also considered the application of a constant axial load. The axial load was applied using three steel transference beams connected by two high-strength rods (Figure 2b). The bottom steel beams were bolted to the concrete strong floor by two ϕ36 mm high-strength steel rods. The rods passed through two hydraulic jacks that reacted against a steel plate and pushed the top transference steel beam against the top beam of the wall.

Instrumentation registered loads, global and local displacements, and strains. The lateral load was captured by the built-in load cell of the hydraulic actuator. The axial load was registered through a load cell placed under the top steel transference beam. Global and local displacements were caught by twenty-three displacement transducers. In this paper, the target displacement (δ_t) is defined as the theoretical displacement intended to be applied to the walls. The actuator and wall displacements, δ_{act} and δ, are those measured by the linear variable differential transducers (LVDT) 23 and 14 (Figure 3), respectively. The location of the displacement transducers is shown in Figure 3(a). Axial strains of the steel reinforcement (rebar) were capture by ten strain gauges (SG) (Tokyo Sokki YFLA-10). The SG were placed in Level 1 and Level 2, 150 mm, and 500 mm apart from the top of the base of the wall, respectively (Figure 3b). Level 1 contained eight SG over the longitudinal bars, and Level 2 comprised two SG placed on the horizontal web reinforcement.

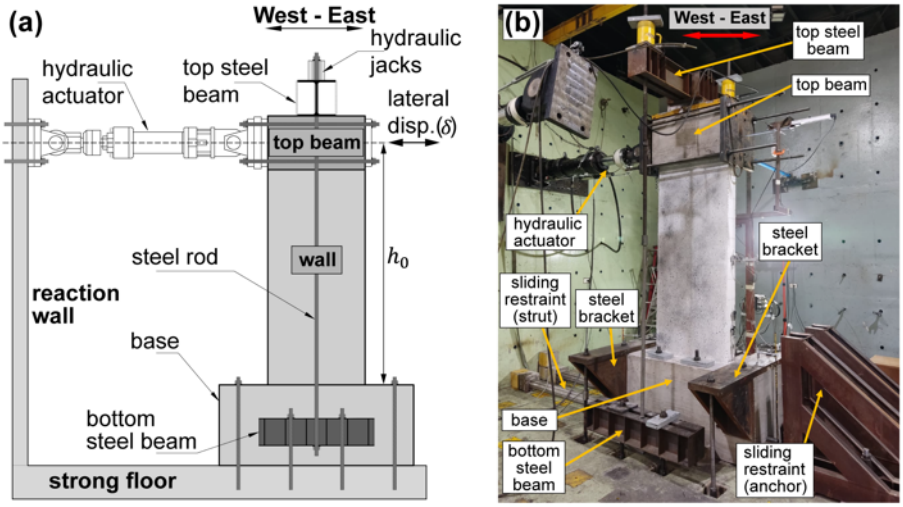

Figure 2. Experimental setup: (a) Elevation, (b) General view of the experimental setup. West-to-east direction means pushing of actuator and positive displacements.

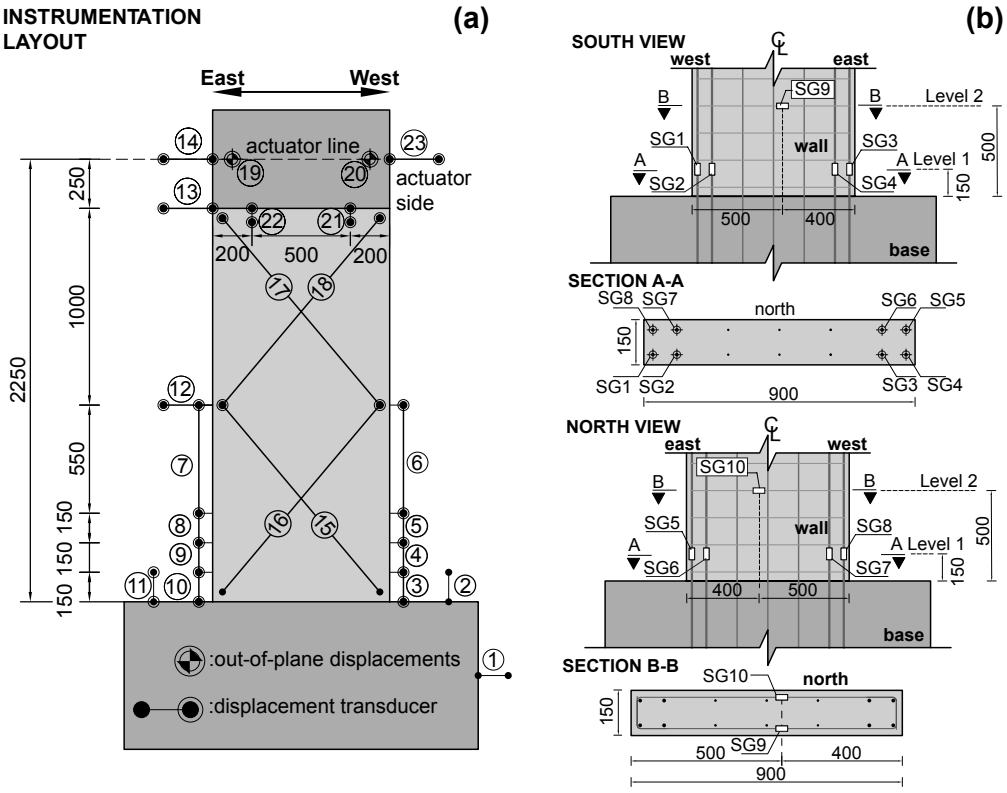

Figure 3. Test instrumentation: (a) displacement transducers layout, (b) strain gauge's location.

Loading protocols

Two loading protocols were applied to the RC wall specimens, a Damage Loading Protocol (DLP) and a Failure Loading Protocol (FLP), Figure 4. The DLP consisted of thirty cycles at constant target drift ratio. The target drift ratio (Δ_t) is defined as δ_t/h_0, being h_0 the distance from the top of the base (foundation) to the actuator axis line (Figure 2a). The DLP's target drift ratios were ±1.33%, ±1.66% and, ±2.00%, for RCW1.33, RCW1.66, and RCW2.00, respectively (Figure 4a-c). Figure 4(a) shows the two loading protocols applied to RCW1.33, where the first thirty cycles at ±1.33% drift correspond to the DLP,

and the remaining cycles correspond to the FLP. Figures 4(b) and (c) show the loading history applied to RCW1.66, and RCW2.0, respectively. RCW2.0 was not loaded with the FLP because the wall failed during the application of the DLP.

The RCW0 was the benchmark wall and was not subjected to a DLP (Figure 4d). The FLP was a quasi-static increasing loading protocol, following ACI 374.2R [22], and consisted of three cycles series of equal drift amplitude. The drift was increased by 0.33%, which corresponded to approximately the drift at yielding of the longitudinal rebar (~0.3%). The lateral loading protocols were applied with a constant axial load of $0.10A_g f_c'$, where A_g is the gross cross-sectional area of the wall, and f_c' is the concrete compressive strength at the age of the tests (29.6 MPa).

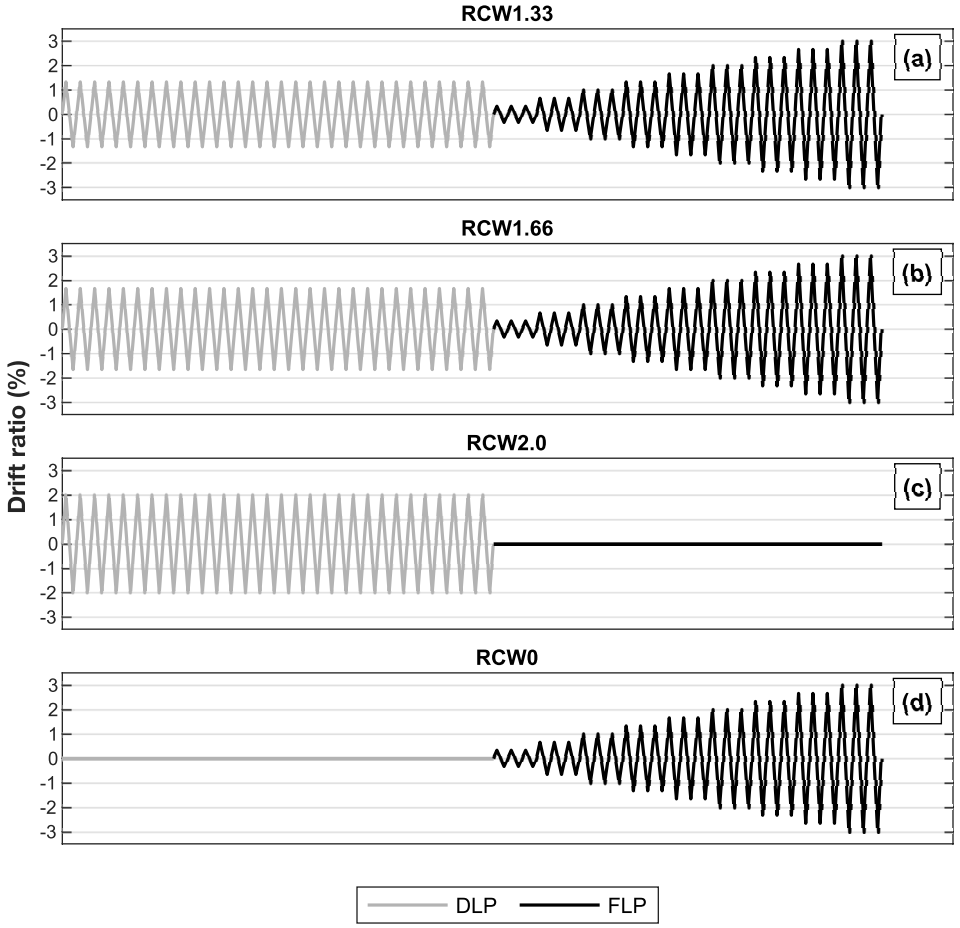

Figure 4. Loading protocols applied to the walls: (a) RCW1.33, (b) RCW1.66, (c) RCW2.0, (d) RCW0.

RESULTS AND DISCUSSION

Observed damaged

Three walls were subjected to a DLP, RCW1.33, RCW1.66 and RCW2.0. RCW1.33 showed similar cracking pattern for the first and last cycle of the DLP, with peak target drifts of ±1.33%. Figure 5(a) shows RCW1.33 at the end of the DLP, where insignificant to slight damage is observed. Figure 5(b) shows that RCW1.66 developed moderate to heavy damage during the DLP, including diagonal shear cracks and spalling plus loss of cover concrete. The vertical extension of the concentrated damage was equivalent to ~30% of the wall length (L_w), Figure 5(b). Finally, RCW2.0 exhibited heavy damage after the DLP, comprising spalling plus loss of the cover concrete, buckling of longitudinal reinforcement, crushing of concrete core and, fracture of longitudinal bars. Subsequently, the wall failed before completing the DLP. Figure 5(c) shows the severe damage accumulated by RCW2.0 during the DLP, covering ~40% L_w.

Three walls (RCW1.33, RCW1.66, and RCW0) were subjected to the FLP. The flexural-compressive behavior controlled the failure of the walls, typical for specimens with similar shear-to-span ratios [9], [15], [16]. The extension of the damaged area in the walls was visibly affected by the prior damage protocols. The damaged areas at the end of the FLP were 0.55 and 0.50 L_w for RCW1.33 and RCW1.66, respectively (Figure 5 d-e). The latter percentages represented plastic hinge length increments

of 66% and 51% with respect to the 0.33 L_w observed for the undamaged RCW0 (Figure 5f). Finally, the observed damaged for RCW0 comprised diagonal cracks with inclination angles ranging from 25° to 50° and horizontal flexural cracks ~200 mm spaced from each other along the base of the wall. The spalling and loss of cover concrete occurred in the FLP third cycle at 1.66% and in the first cycle at 2.33% drift, respectively. The longitudinal rebar buckled in the second cycle of the FLP at 2.66% target drift. The failure of RCW0 was controlled by the crushing of concrete in compression.

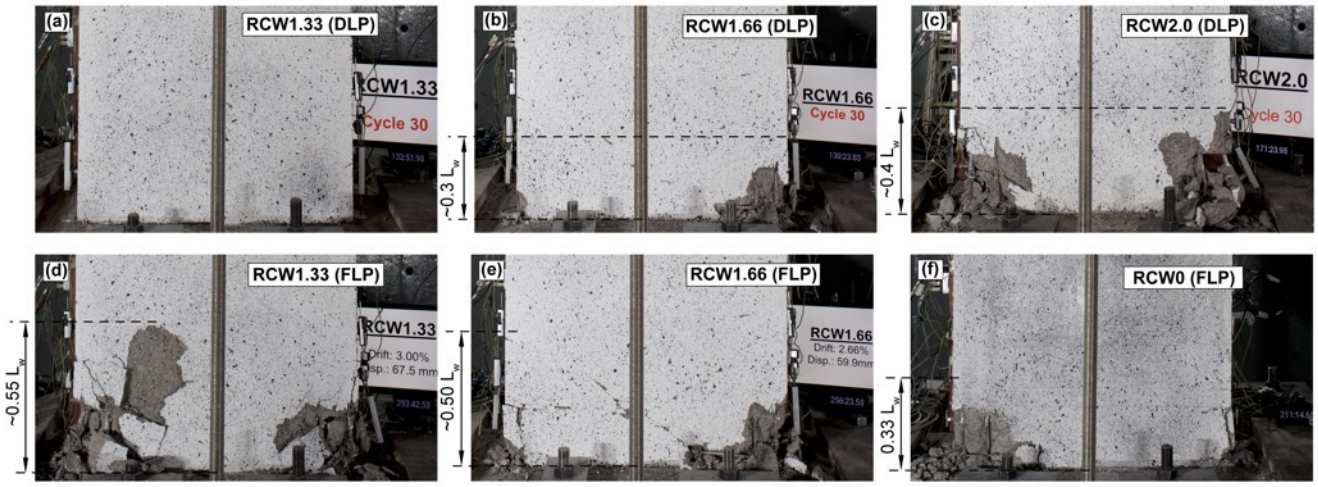

Figure 5. Observed damage in the walls at the end of the loading protocols (Left side of the walls corresponds to the west).

Load-displacement and backbone curves

The effective lateral load-displacement (L-D) curves are shown in Figure 6. These curves were assembled with the history of lateral load and wall displacements (δ), recorded by the load cell of the actuator and LVDT 14, respectively (Figure 3). The actuator displacements were recorded by LVDT 23 (Figure 3). The RCW1.33 L-D relationships for the combined DLP and FLP are presented in Figure 6(a). In general, RCW1.33 showed relatively narrow hysteretic loops during the DLP, with minor loading and un-loading stiffness in comparison with the first loop of this protocol. Regarding the FLP, RCW1.33 showed a generally symmetric hysteretic behavior, with increasingly larger loops as the drift and number of cycles of the protocol increased.

The RCW1.66 L-D relationships for the DLP and FLP are shown in Figure 6(b). The hysteretic behavior of this wall was accordant with the evolution of the damaged observed during its DLP. The last ten hysteretic loops of the RCW1.66 during the DLP exhibited pinching effect (Figure 6b). During the FLP, RCW1.66 showed an asymmetrically hysteric behavior with increasingly larger loops as the drift and number of cycles increased (Figure 6b). In this case, the wall portrayed a rapidly increasing cyclic pinching behavior during the whole FLP, being notorious for the general narrow shape of the hysteric loops.

The RCW2.0 actuator and effective L-D relationships during the DLP are shown in Figure 6(c). The first hysteretic loop of the DLP is not presented in this figure. This setback was caused by an electronic problem with the data acquisition system that prevented it from recording the first cycle of the loading history. The rest of the hysteretic response comprised narrow effective loops that showed pinching effect from the second to the last cycle of the DLP (Figure 6c).

The effective hysteretic response of the benchmark RCW0 is shown in Figure 6(d), showing increasing hysterical loops as the loading protocol advanced. In general, the hysterical loops started presenting pinching behavior in the un-loading branch of the third cycle at +1.26% wall drift, which coincided with the drift at spalling of cover concrete. The pinching effect incremented as the protocol advanced, making the loops narrower cycle-to-cycle until the end of the FLP (Figure 6d).

The backbone curves were constructed from the effective L-D relationships of the FLP applied on RCW1.33, RCW1.66 and RCW0. A preliminary multilinear backbone curve (raw backbone) was drawn for each specimen. This raw backbone connected the peak strength points of the FLP hysteresis through linear segments. The raw multilinear backbones for RCW1.33, RCW1.66, and RCW0 are shown in Figures 6(a), (b) and (d), respectively. No backbone was drawn for RCW2.0 because it was not subjected to the FLP.

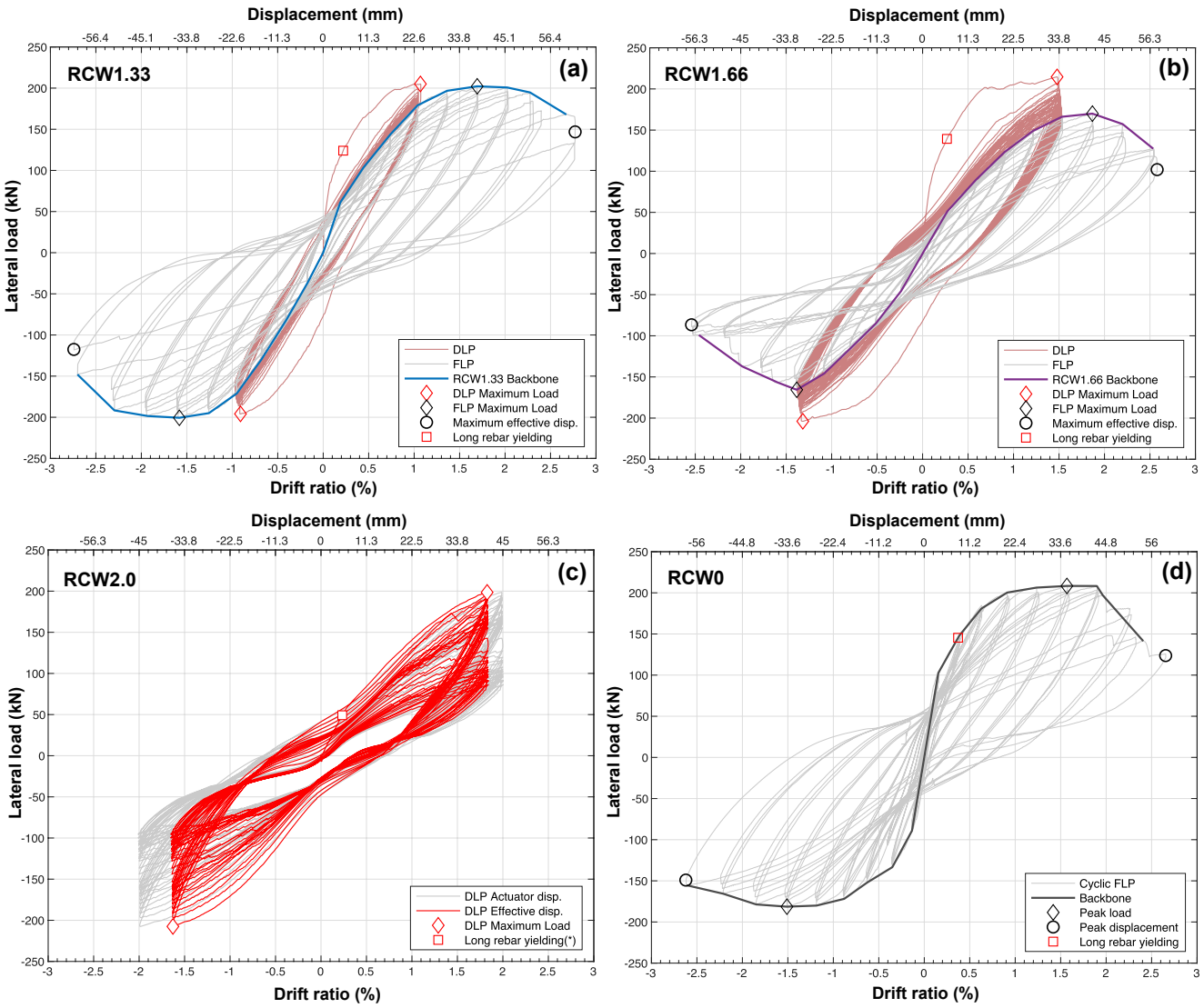

Figure 6. Load-displacement relationships and backbones: (a) RCW1.33, (b) RCW1.66, (c) RCW2.0† and, (d) RCW0. †: the RCW2.0 backbone was not constructed. Positive direction means west-to-east direction or pushing of the hydraulic actuator.

Residual Seismic Capacity

In this paper, the RSC of the damaged walls was estimated through the FEMA component modification factors obtained from the idealized L-D relationships. These idealized relationships were constructed following ASCE 41-17 recommendations [23]. The idealized L-D relationships for RCW0, RCW1.33 and RCW1.66 are presented in Figure 7(a), (b) and (c), respectively. Finally, a comparison between the idealized L-D relationships is shown in Figure 7(d).

The FEMA component modification factors i.e., λ_K, λ_Q and λ_D [24], were estimated using the initial stiffness (K'_e), peak strength (Q'_{max}), and ultimate displacement (δ'_u) from the idealized L-D relationships. The effective stiffness modification factor (λ_K) was calculated as $\lambda_K = K_e'^D / K_e'^U$, where $K_e'^D$ and $K_e'^U$ are the effective stiffness of the damaged and undamaged specimen (RCW0), respectively. The modification factor of the peak strength (λ_Q) was computed as $\lambda_Q = Q'^D_{max} / Q'^U_{max}$, where Q'^D_{max} and Q'^U_{max} are the peak strengths from the idealized curves for the damaged and undamaged wall, respectively. The modification factor of the displacement capacity was computed as $\lambda_D = (\delta_u'^D + R_D)/\delta_u'^U$, where $\delta_u'^D$ and $\delta_u'^U$ are the ultimate displacement from the idealized L-D curves of the damaged and undamaged wall, respectively, and R_D is the absolute value of the residual drift [24], [15]. A summary of the values from the idealized L-D relationships and modification factors of the damaged walls are shown in Table 2 and Table 3, respectively.

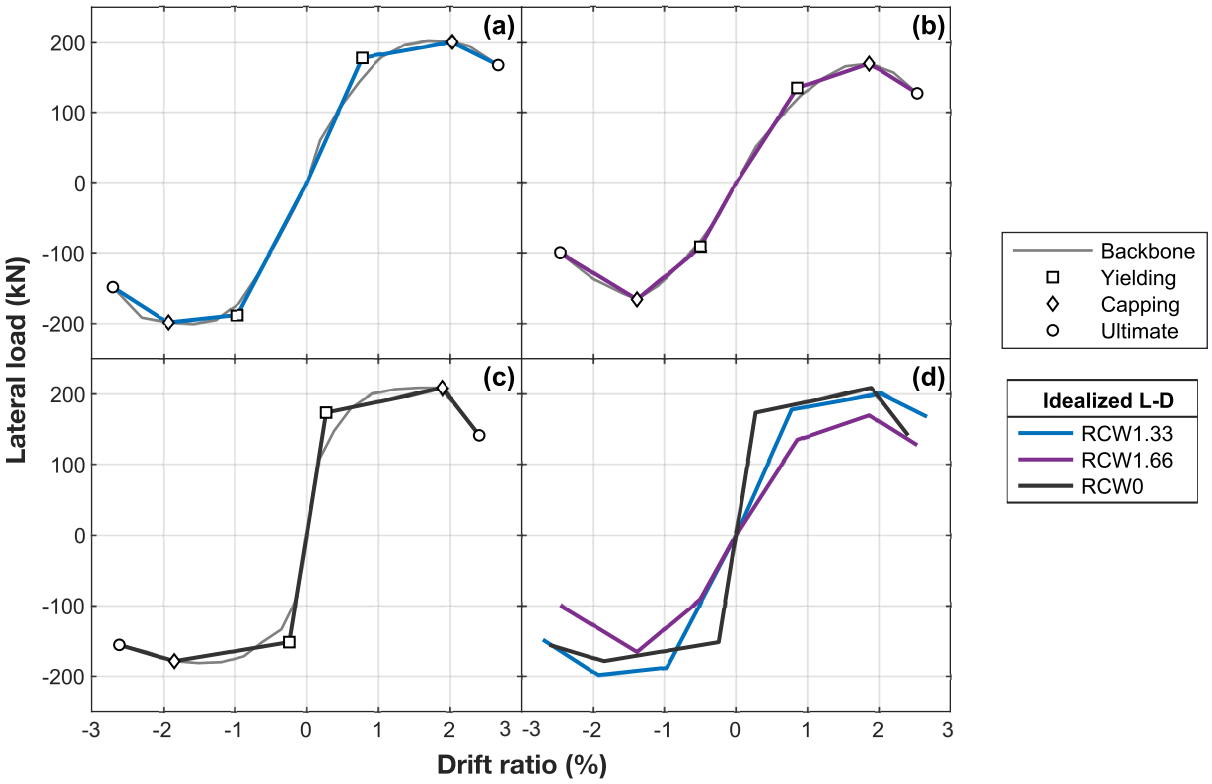

Figure 7. Idealized L-D relationships and backbone curves: (a) RCW1.33, (b) RCW1.66, (c) RCW0 and, (d) Comparison of the idealized L-D for the wall specimens.

Table 2. Notable values from the idealized L-D relationships of the walls subjected to the DLP and FLP.

Idealized L-D point	id	RCW1.33	RCW1.66	RCW0
Effective stiffness	$K_e'^{\dagger}$ (kN/mm)	10.12	6.97	28.54
	$K_e'^{ß}$ (kN/mm)	8.58	8.09	28.18
Capping point	Q'^{+}_{max} (kN)	202	170	208
	Q'^{-}_{max} (kN)	-201	-166	-181
Ultimate point	Δ'^{+}_{u} (%)	2.67	2.54	2.41
	Δ'^{-}_{u} (%)	-2.7	-2.46	-2.61
	Q'^{+}_{u} (kN)	168	127	141
	Q'^{-}_{u} (kN)	-148	-99	-155
Average displacement Ductility	μ' (%)	3.1	3.9	9.9

†, ß: effective stiffness of the positive and negative branches of the idealized L-D relationships, respectively. μ': average ductility from the idealized L-D relationship (Δ'_u/Δ'_y).

Table 3. Component modification factors for the damaged walls.

Specimen	λ_K	λ_Q	RD (%)	λ_D
RCW1.33	0.33	1.04	0.16	1.01
RCW1.66	0.27	0.86	0.26	0.89

CONCLUSIONS

An experimental campaign was conducted to evaluate the RSC of damaged rectangular, slender, and unconfined RC walls. Four specimens were built and tested on laboratory, RCW1.33, RCW1.66, RCW2.0 and RCW0. Specimens RCW1.33, RCW1.66, and RCW2.0 were previously loaded with a DLP, consisting of thirty cycles at $\pm$1.33%, $\pm$1.66% and $\pm$2.0% target drift ratios, respectively. Subsequently, a standard FLP was applied to RCW1.33 and RCW1.66 until failure. RCW2.0 was not subjected to the FLP because it failed during the DLP. RCW0 (benchmark) was only subjected to the FLP in undamaged condition. After estimating of the RSC of the damaged walls, the following conclusions derives,

- The amplitude of the DLP previous cycles controlled the level of visual damage of the studied specimens. The DLP with thirty cycles at 1.33% target drift produced slight damage to RCW1.33. Neither vertical cracks on wall boundary regions nor spalling of the cover concrete were reported at the end of this protocol. The DLP at 1.66% target drift produced moderate to heavy damage on RCW1.66. Visual damaged comprised diagonal shear cracks, spalling plus loss of cover concrete and buckling of longitudinal rebar at the end of the DLP. Few cycles of the DLP at 2.0% target drift ratio produced heavy damage to RCW2.0, being just three and six cycles of the DLP enough to cause spalling and loss of cover concrete, respectively.
- DLPs with thirty cycles that at least quadrupled the drift at first yielding of the longitudinal reinforcement (0.3%), affected the RSC of the studied walls. RCW1.33 reported a 67% reduction of the effective stiffness (K_e) compared to RCW0. However, there were no peak strength and deformation capacity reduction for RCW1.33. Also, the displacement ductility (μ) for RCW1.33 plumped 68% compared to RCW0. Compared to RCW0, RCW1.66 lost 73% and 13% of its effective stiffness and peak strength, respectively. There was no loss in deformation capacity reported for this specimen. However, the displacement ductility plumped approximately 60%.

ACKNOWLEDGMENTS

This research was carried out with the financial support provided by ANID/FONDECYT through grant No. 1211823. The authors would like to acknowledge the support of ANID/FONDAP/1522A0005 (National Research Center for the Integrated Management of Natural Disasters, CIGIDEN). Edgar Chacón-Valero acknowledges the financial support of the scholarship ANID/Doctorado Nacional 2019/21190644. Special thanks to the PhD. (c) Luis Pérez for the logistical support during the experimental campaign.

REFERENCES

[1] J. W. Wallace *et al.*, "Damage and implications for seismic design of RC structural wall buildings," *Earthquake Spectra*, vol. 28, no. SUPPL.1, pp. 281–299, 2012, doi: 10.1193/1.4000047.

[2] F. Marquis, J. J. Kim, K. J. Elwood, and S. E. Chang, "Understanding post-earthquake decisions on multi-storey concrete buildings in Christchurch, New Zealand," *Bulletin of Earthquake Engineering*, vol. 15, no. 2, pp. 731–758, 2017, doi: 10.1007/s10518-015-9772-8.

[3] S. Alcocer *et al.*, "Observations about the seismic response of RC buildings in Mexico City," *Earthquake Spectra*, vol. 36, no. 2_suppl, pp. 154–174, Dec. 2020, doi: 10.1177/8755293020942523.

[4] M. E. Rodriguez, "The interpretation of cumulative damage from the building response observed in Mexico City during the 19 September 2017 earthquake," *Earthquake Spectra*, vol. 36, no. 2_suppl, pp. 199–212, Dec. 2020, doi: 10.1177/8755293020971307.

[5] L. Dal Zilio and J.-P. Ampuero, "Earthquake doublet in Turkey and Syria," *Commun Earth Environ*, vol. 4, no. 1, p. 71, Mar. 2023, doi: 10.1038/s43247-023-00747-z.

[6] K. J. Marder, K. J. Elwood, and G. C. Clifton, "Post-earthquake residual capacity of damaged reinforced concrete buildings," in *Proceedings of the 16th World Conference on Earthquake Engineering (16WCEE), Santiago, Chile*, 2017.

[7] J. S. Kuang and Y. B. Ho, "Seismic Behavior and Ductility of Squat Reinforced Concrete Shear Walls with Nonseismic Detailing," *ACI Struct J*, vol. 105, no. 2, pp. 225–231, 2008.

[8] C. Alarcon, M. A. Hube, and J. C. de la Llera, "Effect of axial loads in the seismic behavior of reinforced concrete walls with unconfined wall boundaries," *Eng Struct*, vol. 73, pp. 13–23, Aug. 2014, doi: 10.1016/j.engstruct.2014.04.047.

[9] M. A. Hube, A. Marihuén, J. C. de la Llera, and B. Stojadinovic, "Seismic behavior of slender reinforced concrete walls," *Eng Struct*, vol. 80, pp. 377–388, Dec. 2014, doi: 10.1016/j.engstruct.2014.09.014.

[10] Y. Lu, R. S. Henry, Ronald Gultom, and Q. T. Ma, "Cyclic Testing of Reinforced Concrete Walls with Distributed Minimum Vertical Reinforcement," *J. Struct. Eng.*, vol. 143, no. 5, pp. 1–17, 2016, doi: 10.1061/(ASCE)ST.1943.

[11] F. Dashti, R. P. Dhakal, and S. Pampanin, "Tests on Slender Ductile Structural Walls Designed According to New Zealand Standard" *Bulletin of the New Zealand Society for Earthquake Engineering*, vol. 50, no. 4, 2017.

[12] C. L. Segura and J. W. Wallace, "Seismic performance limitations and detailing of slender reinforced concrete walls," *ACI Struct J*, vol. 115, no. 3, pp. 849–859, May 2018, doi: 10.14359/51701918.

[13] A. V. Shegay, C. J. Motter, K. J. Elwood, R. S. Henry, D. E. Lehman, and L. N. Lowes, "Impact of Axial Load on the Seismic Response of Rectangular Walls," *Journal of Structural Engineering (United States)*, vol. 144, no. 8, 2018, doi: 10.1061/(ASCE)ST.1943-541X.0002122.
[14] T. Zhang, "Seismic Assessment of Singly Reinforced Concrete Walls in Pre-1970s Multi-Storey Buildings," PhD Thesis, The University of Auckland, Auckland, 2020.
[15] J. F. Moscoso, M. A. Hube, and H. S. María, "Residual seismic capacity of reinforced concrete walls with unconfined boundaries," *ACI Struct J*, vol. 118, no. 5, pp. 205–220, Sep. 2021, doi: 10.14359/51732830.
[16] J. Colmenares, H. Santa María, and M. Hube, "Effect of the Number of Cycles on the Seismic Residual Capacity of Slender RC Structural Walls with Unconfined Boundaries," 2022.
[17] H. Alwashali, M. Maeda, Y. Ogata, N. Aizawa, and K. Tsurugai, "Residual seismic performance of damaged reinforced concrete walls," *Eng Struct*, vol. 243, Sep. 2021, doi: 10.1016/j.engstruct.2021.112673.
[18] ASTM C469/469M, "ASTM C469/469M. Standard Test Method for Static Modulus of Elasticity and Poisson's Ratio of Concrete in Compression." ASTM Inernational: West Conshohocken, PA, USA, 2014.
[19] NCh204, *NCh204.Of2006 Acero - Barras laminadas en caliente para hormigón armado*, Primera edición:2006. Santiago, Chile: Instituto Nacional de Normalización, 2006.
[20] NCh200, *NCh200.Of1972 Productos Metálicos - Ensayo de tracción*, Reimpresión: 1999., vol. 1. Santiago, Chile: Instituto Nacional de Normalización, 1972.
[21] J. Amón, "Estudio Experimental del Comportamiento Sísmico y La Capacidad Residual en Muros Esbeltos de Hormigón Armado," Magister Thesis, Pontificia Universidad Católica de Chile, Santiago de Chile, 2018.
[22] ACI 374.2R, *Guide for Testing Reinforced Concrete Structural Elements Under Slowly Applied Simulated Seismic Loads*. American Concrete Institute (ACI), 2013.
[23] ASCE/SEI 41, *Seismic Evaluation and Retrofit of Existing Buildings*. Reston, Virginia: American Society of Civil Engineers, 2017.
[24] FEMA, *306 Evaluation of Earthquake Damaged Concrete and Masonry Wall Buildings: Basic Procedures Manual (FEMA 306)*. Applied Technology Council, 1998.